PROTEIN STRUCTURE REPORT

Solution structure of the N-terminal A domain of the human voltage-gated Ca^{2+} channel β_{4a} subunit

ANDREW C. VENDEL,[1] CHRISTOPHER D. RITHNER,[2] BARBARA A. LYONS,[3] AND WILLIAM A. HORNE[1]

[1]Department of Biomedical Sciences, College of Veterinary Medicine and Biomedical Sciences, and [2]Department of Chemistry, College of Natural Sciences, Colorado State University, Fort Collins, Colorado 80526, USA
[3]Department of Chemistry and Biochemistry, College of Arts and Sciences, New Mexico State University, Las Cruces, New Mexico 88003, USA

(RECEIVED October 7, 2005; FINAL REVISION November 4, 2005; ACCEPTED November 8, 2005)

Abstract

Ca^{2+} channel β subunits regulate trafficking and gating (opening and closing) of voltage-dependent Ca^{2+} channel α_1 subunits. Based on primary sequence comparisons, they are thought to be modular structures composed of five domains (A–E) that are related to the large family of membrane associated guanylate-kinase (MAGUK) proteins. The crystal structures of the β subunit core, B–D, domains have recently been reported; however, very little is known about the structures of the A and E domains. The N-terminal A domain is a hypervariable region that differs among the four subtypes of Ca^{2+} channel β subunits (β_1–β_4). Furthermore, this domain undergoes alternative splicing to create multiple N-terminal structures within a given gene class that have distinct effects on gating. We have solved the solution structure of the A domain of the human β_{4a} subunit, a splice variant that we have shown previously to have α_1 subunit subtype-specific effects on Ca^{2+} channel trafficking and gating.

Keywords: Ca^{2+} channel; β_{4a} subunit; nuclear magnetic resonance; alternative splicing; membrane-associated guanylate-kinase protein; protein structure; domains and motifs; exon/intron relationship; ion channel

Voltage-gated Ca^{2+} channels open in response to membrane depolarizations induced by propagating action potentials and thereby regulate excitation–contraction coupling in skeletal and heart muscle cells and excitation-transmitter release coupling in neurons (Catterall 2000). Their influence over cytosolic Ca^{2+} levels also gives them a prominent role in Ca^{2+}-mediated signal transduction and gene expression. Voltage-gated Ca^{2+} channel complexes include four subunits, α_1, α_2/δ, and β, that are assembled in a 1:1:1:1 ratio (Dalton et al. 2005). Ten genes code for α_1 subunits (180–240 kDa) and are classified into three main families, Ca_v1–Ca_v3. The α_1 subunit forms the pore and can function without α_2/δ and β; however, the gating properties of α_1 subunits alone do not match those of native channels. Four genes code for α_2/δ subunits (~150 kDa), consisting of two proteins attached by multiple disulfide bonds (Arikkath and Campbell 2003). The δ subunit is inserted into the plasma membrane, while the heavily glycosylated α_2 subunit is entirely extracellular. In contrast, β subunits, encoded by four genes, β_1–β_4, are located on the cytosolic surface of the complex and bind to a well-characterized inter-

Reprint requests to: William A. Horne, Department of Biomedical Sciences, 1617 Campus Delivery, Colorado State University, Fort Collins, CO 80523, USA; e-mail: bill.horne@colostate.edu; fax: (970) 491-7907.

Abbreviations: AID, α_1 subunit interaction domain; DSS, 2-2-Dimethyl-2-silapentane-5-sulfonic acid; GK, guanylate-kinase; HSQC, heteronuclear single quantum coherence; MAGUK, membrane associated guanylate-kinase; NMR, nuclear magnetic resonance; NOE, nuclear Overhauser effect; NOESY, NOE spectroscopy; PCR, polymerase chain reaction; RMSD, root-mean-square deviation; SH3, src homology 3; TOCSY, total correlation spectroscopy.

Article published online ahead of print. Article and publication date are at http://www.proteinscience.org/cgi/doi/10.1110/ps.051894506.

action domain (AID) on the intracellular loop of α_1 subunits (Pragnell et al. 1994; Richards et al. 2004). The β subunits mediate α_1/α_2 trafficking and surface expression and regulate gating kinetics via multiple contacts with the α_1 subunit (Maltez et al. 2005).

The β subunits contain five proposed structural domains (A–E) (Hanlon et al. 1999). These domains show striking similarity to a number of membrane-associated guanylate kinase (MAGUK) proteins (McGee et al. 2004), indicating that they have evolved from a common ancestor. Based on X-ray crystallography (Chen et al. 2004; Opatowsky et al. 2004; Van Petegem et al. 2004) and sequence alignments with MAGUK proteins (McGee et al. 2004), the B domain (~66 residues) resembles an SH3 fold, and the D domain (~190 residues), a guanylate-kinase fold. These domains form the core structure of the β subunit. Primary sequence alignments of the different β subunits indicates a high level of conservation in the core SH3 (>60%) and GK (>67%) domains, suggesting that the core domain has similar functions in all β subunits. The hypervariable A, C, and E domains are not well-conserved between β subunit subtypes and undergo extensive alternative splicing. It is likely that these variable domains serve cell-type and α_1 subunit-specific roles in regulating Ca^{2+} channel function.

We have shown previously that the β_4 subunit undergoes alternative splicing to generate A domains of either 58 (β_{4a}) or 92 (β_{4b}) residues that precede the SH3 fold (Helton and Horne 2002). Functional studies indicate that this alternative splicing event results in differential gating of P/Q type Ca^{2+} channels (Helton et al. 2002). To date, only the SH3 and GK domains have been shown to bind directly to the α_1 subunit (Maltez et al. 2005), raising the possibility that β subunit A domains may regulate channel properties through protein–protein interactions with non-Ca^{2+} channel proteins. To further understand the role of the β subunit A domain in Ca^{2+} channel gating and synaptic transmission, we determined the three-dimensional solution structure of the β_{4a}-A domain. Our results show that the β_{4a}-A domain is an independently folded module positioned away from the β subunit core and α_1 subunit and support the idea that the β_{4a}-A domain is involved in protein–protein interactions.

Results

Structure of the human Ca^{2+} channel β_{4a}-A domain

The sequence and predicted secondary structure of the β_{4a}-A domain are aligned in Figure 1A. The prediction indicates that the A domain contains 2 α-helices and 2 β-strands. Nuclear magnetic resonance (NMR) spectroscopic methods were used to determine the high-resolution three-dimensional structure of the protein. Sequence-specific chemical shift assignments of β_{4a}-A were accomplished using standard triple-resonance experimental procedures outlined in the Materials and Methods section. The locations of secondary structural elements were identified by chemical shift indices, H^NH^α coupling constants, and NOE interaction patterns (Fig. 1B). Based on NOESY and dihedral angle restraint data (H^NH^α coupling constants), and in agreement with the secondary structure prediction, the β_{4a}-A domain is composed of two anti-parallel β-sheets (residues 19–22 and 26–29) and two α-helices (residues 2–7 and 40–55). These results and preliminary NOE constraint data were used to generate a number of hydrogen bonds used in the final structure calculations of the β_{4a}-A domain.

The β_{4a}-A domain solution structure (Fig. 1C) reveals that the short N-terminal helix (α1) packs against the conserved C-terminal helix (α2). Between the two helices there are three loop structures (L1, L2, and L3) and a pair of short, anti-parallel β-strands (β1 and β2). The first helix (α1) is positioned orthogonal to the second helix (α2) and is packed between α2 and the β elements. Tyr21 of β1 packs against Leu5, Tyr6, and Leu7 on α1 to create a small hydrophobic core for the β_{4a}-A domain.

The C-terminal helix (α2) shown in the NMR structure corresponds to the N-terminal helix of the β_{2a} core (SH3-GK) X-ray crystal structure (Opatowsky et al. 2004). In this helix, Glu44, Ala47, Gln50, Leu51, Ala54, and Lys55 of β_{4a} are conserved in all β subunits. The β_{2a} crystal structure indicates that these residues make contacts with a surface distal to the canonical SH3 PXXP binding pocket (Fig. 1D). The conservation of these residues on α2 of the A domain suggests that these residues are likely important for stabilizing the A domain and orienting it away from the Ca^{2+} channel α_1 subunit interaction domain (AID).

A total of 1156 restraints were used to calculate a family of 15 representative structures (Fig. 2) with a root-mean-square deviation (RMSD) of 0.74 Å for the backbone atoms and 1.35 Å for all atoms (Table 1). Ramachandran plot analysis of the secondary elements of the β_{4a}-A domain yields 79% of residues in most favored regions, 16.3% in additional allowed regions, 4.7% in generously allowed regions, and 0% in disallowed regions. Further statistical information for the set of 15 structures of the β_{4a}-A domain is found in Table 1. Atomic coordinates for the human β_{4a}-A domain have been deposited with the protein database (PDB) at Rutgers University (accession code 2D46). Structural analysis using several PDB programs revealed that the β_{4a}-A domain has a unique fold.

Discussion

The structures of Ca^{2+} channel β subunits have eluded investigators for >15 yr following the cloning and

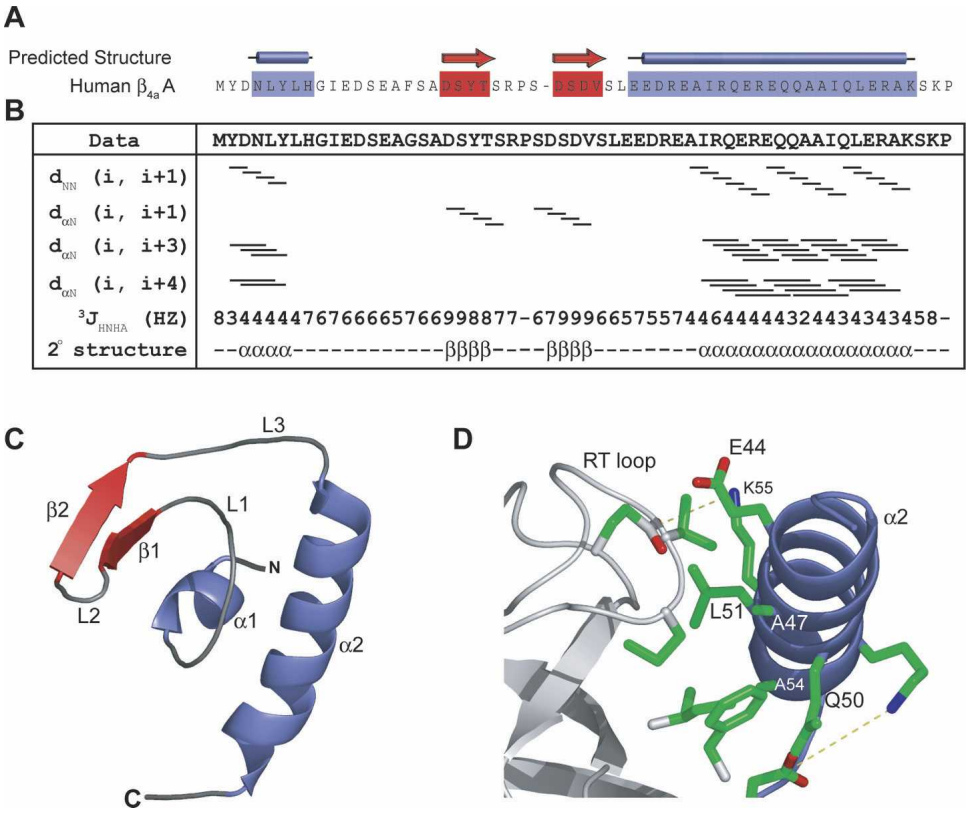

Figure 1. (*A*) Secondary structure predictions performed with the PSA server (http://bmerc-www.bu.edu/psa; White et al. 1994) indicate that the β_{4a}-A domain has a mixture of α-helix and β-sheet. (*B*) Secondary structural characterization by multi-dimensional NOESY-HSQC and HNHA J coupling experiments. Solid bars for d_{NN} (*i*, *i* + 1) and $d_{\alpha N}$ (*i*, *i* + 1) represent continuous cross peaks observed in ^{15}N-edited NOESY-HSQC experiments run with a 50-msec mixing time. Lines for $d_{\alpha N}$ (*i*, *i* + 3) and $d_{\alpha N}$ (*i*, *i* + 4) represent NOE cross-peaks between residues three and four amino acids away, respectively. The $^{3}J_{HNHA}$ coupling constants provide further information on the secondary structure boundaries. These results outline the secondary structural elements present in the β_{4a}-A domain and correlate with predicted structural elements. (*C*) Solution structure of the β_{4a}-A domain determined with a backbone RMSD of 0.73 Å (Table 1). The β_{4a}-A domain is independently folded with the first helix (α1) coordinating two β-strands (β1 and 2), three loops (L1–3), and a C-terminal α-helix (α2) to create a globular, hydrophobic core. (*D*) The α2 helix is involved in packing against the SH3 domain (Opatowsky et al. 2004). Conserved residues are involved in hydrophobic packing (A54, L51, and A47 on the A domain, and V80, F100, W104, and I106 on the SH3 domain) and formation of salt bridges (R53–E97 and K55–E115) between the A and the SH3 domains of β_{4a}.

sequencing of the first skeletal muscle β_1 subunit (Ruth et al. 1989). Progress toward solving their structures began only when it was recognized that these proteins were members of the large family of modular MAGUK proteins (Hanlon et al. 1999). Post-synaptic-density protein 95 (PSD-95) served as a model for approaching the structure of β subunits. The X-ray crystal structure of the core SH3 and GK domains of PSD-95 was solved after removing its three N-terminal PDZ domains (McGee et al. 2001). A similar approach proved successful in solving the crystal structures of the core SH3 and GK domains of Ca^{2+} channel subunits β_{2a}, β_3, and β_4 (Chen et al. 2004; Opatowsky et al. 2004; Van Petegem et al. 2004). Difficulties in crystallizing full-length β subunits likely arise from the dynamic structures of the N-terminal A and C-terminal E domains. This is supported by the fact that in the present study low temperatures were used to stabilize the β_{4a}-A domain fold and to provide better resolved data. Circular dichroism studies of the β_{4a}-A domain reveal a partial unfolding of the structure with increasing temperature (A. Vendel, unpubl.). This may be due to loss of stabilizing interactions of the α_2 helix with the SH3 domain present in the native β_{4a} structure (Fig. 1D). However, yeast two-hybrid studies carried out at 30°C indicate that the β_{4a}-A domain is capable of protein–protein interactions (N. Iverson, unpubl.), suggesting that the conformation of the A domain could be stabilized through protein–protein interactions. Our ongoing studies are addressing these possibilities.

This is the first report showing that residues in a domain outside the core of the Ca^{2+} channel β subunit are capable of independent folding. This is especially interesting in light of the fact that these are the regions

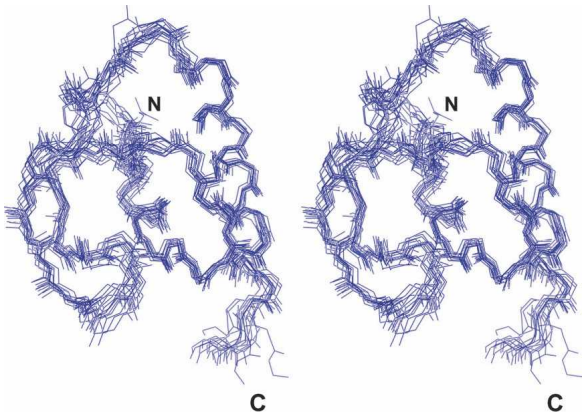

Figure 2. Stereo view of the 15 lowest energy solution structures of the human Ca^{2+} channel β_{4a} subunit A domain. Shown are the backbone traces of the β_{4a}-A domain with the highest convergence in the structured residues 2–7 (α1), 19–22 (β1), 26–29 (β2), and 40–55 (α2).

that undergo alternative splicing. It has become increasingly apparent in recent years that alternative splicing, especially in the nervous system, has evolved to increase the number of unique proteins from what is a surprisingly limited gene pool (Lipscombe 2005). The results presented in this protein structure report are an important step toward understanding the structural and functional consequences of one of these alternative splicing events.

Materials and methods

Protein expression and purification

To determine the structure of the β_{4a}-A domain, a PCR fragment encoding residues 1–58 of the full-length human β_{4a} gene (accession no. NP_001005747) was cloned into a bacterial expression vector containing an N-terminal His-tag sequence (pET-15b, Novagen). The resulting construct was sequenced prior to expression and purification. The pET-15b β_{4a}-A expression vector was transformed into *Escherichia coli* strain BL21-CodonPlus (DE3)-RIL (Stratagene). Cells were grown at 37°C to an optical density of 0.6 at 600 nm and induced with 1 mM isopropyl-β-D-thiogalactopyranoside (IPTG) (Anatrace) for 4 h. Cells were harvested by centrifugation and lysed by sonication in 50 mM sodium phosphate, 500 mM NaCl, and 10 mM imidazole (pH 8) (Ni^{2+}-load buffer). Histidine-tagged β_{4a}-A (His-β_{4a}-A) was removed from the soluble fraction by Ni^{2+} affinity chromatography (His·Bind; Novagen), washed with Ni^{2+}-load buffer to remove contaminants, and eluted with 50 mM sodium phosphate, 300 mM NaCl, and 400 mM imidazole (pH 8.4) (Ni^{2+}-elute buffer). Excess imidazole was removed by dialyzing His-β_{4a}-A against 50 mM sodium phosphate, 150 mM NaCl, and 10 mM imidazole (pH 8.4). The His-tag was removed by thrombin cleavage overnight at room temperature. The cleaved His-tag was separated from β_{4a}-A by Ni^{2+} affinity chromatography. The flowthrough containing β_{4a}-A was dialyzed against 50 mM sodium phosphate (pH 7.0) overnight at 4°C, prior to final purification by anion exchange chromatography (UNO Q6 column and Biologic DuoFlow System, BioRad) using a linear salt gradient from 0 to 1 M NaCl. Purified β_{4a}-A was dialyzed against 16 L of water and stored as lyophilized powder. The identity and the purity of the β_{4a}-A domain was confirmed with electrospray mass spectrometry, and the observed and the expected mass agreed to within 1 Da.

^{15}N-labeled and ^{15}N, ^{13}C-labeled β_{4a}-A was prepared as described above, except cells were grown in M9 minimal medium containing 0.8 g/L $^{15}NH_4Cl$ and 3 g/L ^{13}C-glucose (McIntosh and Dahlquist 1990), supplemented with 10% ^{15}N and ^{15}N, ^{13}C-labeled Celtone media (Spectra). The final yield of purified ^{15}N, ^{13}C uniformly labeled β_{4a}-A was 25 mg/L.

Protein concentration determination

Concentrations of protein stock solutions were determined by absorbance in 6 M GuHCl, 10 mM sodium phosphate, and 150 mM sodium chloride (pH 6.5) at 25°C using an extinction coefficient for β_{4a}-A of 4350 M^{-1} cm^{-1} (Edelhoch 1967).

NMR spectroscopy

NMR spectra were acquired with a Varian Unity Inova spectrometer operating at 500.1 MHz for ^1H, 125.7 MHz for ^{15}N,

Table 1. *Summary of structural statistics for the human β_{4a}-A domain, ensemble of the 15 lowest energy structures*

NOE upper distance limits	963
Intraresidue	472
Sequential	196
Medium range ($1 < \|i-j\| \leq 4$)	87
Long range ($\|i-j\| > 4$)	208
Dihedral angle constraints	143
ϕ	52
Ψ	52
χ	39
Hydrogen bonds	2×25
RMSD from experimental constraints	
Distances (Å)	0.0339 ± 0.001
Dihedrals (°)	0.7455 ± 0.134
Average number of NOE distance constraint violations	
> 0.5 Å	0.00 ± 0.00
> 0.2 Å	2.27 ± 1.39
RMSD from idealized covalent geometry	
Bonds (Å)	0.0054 ± 0.0003
Angles (°)	0.6689 ± 0.0333
Impropers (°)	0.6105 ± 0.0426
Atomic RMSD values (Å) for β_{4a}-A domain residues 1–55	
Backbone atoms	0.74 ± 0.11 Å
All atoms	1.35 ± 0.17 Å
Ramachandran plot (%)[a,b]	
Most favored regions	79.0%
Additional allowed regions	16.3%
Generously allowed regions	4.7%
Disallowed regions	0.0%

Structure statistics are reported as averages of the 15 lowest energy structures calculated from the CNS program.
[a] Glycines and prolines are excluded.
[b] Residues 1–11, 19–22, and 27–55.

and 50.6 MHz for ^{13}C. Internal DSS (2,2-dimethyl-2-silapentane-5-sulphonic acid) was used to standardize ^{1}H, ^{15}N, and ^{13}C chemical shifts based on IUPAC recommendations (Wishart and Case 2001). Data were processed with NMRPipe (Delaglio et al. 1995) and analyzed with NMRView (Johnson and Blevins 1994) and ANSIG for Windows (Helgstrand et al. 2000). All spectra were acquired at 5°C on samples prepared in 50 mM sodium phosphate, 150 mM NaCl, 10% D_2O, and 100 μM sodium azide (pH 5.5).

Sequence specific assignments of the β_{4a}-A backbone resonances were obtained using combinations of gradient sensitivity-enhanced HNCA, HN(CO)CA; HNCO, HN(CA)CO; HNCACB and CBCA(CO)NH experiments as described elsewhere (Cavanagh et al. 1996). Sequence-specific side-chain assignments were accomplished with HNCACB, CBCA(CO)NH, ^{15}N-edited HCCONH and TOCSY-HSQC, and ^{13}C-edited HCCH-TOCSY experiments (Cavanagh et al. 1996). Backbone ϕ angles of β_{4a}-A were constrained using the $^{3}J_{HNHA}$ experiment (Kuboniwa et al. 1994) with T_1 and T_2 values of 7.5 and 12.5 msec, respectively. Experiments were run with spectral windows of 6982 and 5500 for ^{1}H in the direct and the indirect dimensions, respectively; 1700 for ^{15}N; and 10,063 for ^{13}C. Linear prediction was applied to all data prior to apodization, zero filling, and Fourier transformation.

Structure determination

A total of 1156 structural restraints were used to calculate the final 15 representative solution structures of the β_{4a}-A domain (Fig. 2). Nine hundred sixty-three NOE derived distance constraints were utilized in the calculation, of which 472 were intraresidue, 196 sequential, 87 medium-range ($4 < |i-j| > 1$), and 208 long-range ($|i-j| \geq 4$) (Table 1), providing an average of 15.8 NOE constraints/residue. NOE cross-peak intensities were classified into three categories: strong (1.8–2.5 Å), medium (2.6–3.5 Å), and weak (3.6–6.0 Å). A total of 104 ϕ and ψ dihedral angle constraints were obtained from a directly measured $^{3}J_{HNHA}$ experiment and the TALOS program (Cornilescu et al. 1999), respectively. Thirty-nine Chi (χ_1) dihedral angles were restrained to one of three values (60°, 180°, −60°) based on measured HNHB coupling constants or αβ2-αβ3/NHβ2-NHβ3 NOE profiles. A total of 25 hydrogen bond restraints were used in structure calculations, based on $^{3}J_{HNHA}$ coupling constants, ^{15}N-edited NOESY-HSQC spectral analysis, and preliminary structure calculations. Structure calculations were performed with Crystallography and NMR System (CNS) (Brunger et al. 1998). Initial high-temperature annealing was set at 50,000 K with 1000 dynamic steps of 15 fsec, and NOE and dihedral scaling factors of 150 and 100, respectively, followed by a primary torsion slow-cooling stage of 1000 steps of 15 fsec with a temperature gradient from 50,000 to 0 K in 250-K increments. A second cartesian slow-cooling stage was performed consisting of 3000 steps of 5 fsec, cooling from 2000 to 0 K. Final minimization consisted of 10 cycles of 200 steps with dihedral angle and NOE energy constants set to 400 and 200 kcal mol^{-1} $Å^{-4}$, respectively.

Acknowledgments

This work was supported by a grant from the NIH (R01 NS42600) to W.A.H. We thank Nicole Iverson for assistance in protein purification, and Ryan McKay (NANUC, Alberta, Canada) and Pascal Mercier (University of Alberta, Canada) for helpful discussions relating to data analysis.

References

Arikkath, J. and Campbell, K.P. 2003. Auxiliary subunits: Essential components of the voltage-gated Ca^{2+} channel complex. *Curr. Opin. Neurobiol.* **13:** 298–307.

Brunger, A.T., Adams, P.D., Clore, G.M., DeLano, W.L., Gros, P., Grosse-Kunstleve, R.W., Jiang, J.S., Kuszewski, J., Nilges, M., and Pannu, N.S. 1998. Crystallography & NMR System: A new software suite for macromolecular structure determination. *Acta Crystallogr. D Biol. Crystallogr.* **54:** 905–921.

Catterall, W.A. 2000. Structure and regulation of voltage-gated Ca^{2+} channels. *Annu. Rev. Cell Dev. Biol.* **16:** 521–555.

Cavanagh, J., Fairbrother, W.J., Palmer III, A.G., and Skelton, N.J. 1996. *Protein NMR spectroscopy: Principles and practice,* p. 597. Academic Press, San Diego, CA.

Chen, Y.H., Li, M.H., Zhang, Y., He, L.L., Yamada, Y., Fitzmaurice, A., Shen, Y., Zhang, H., Tong, L., and Yang, J. 2004. Structural basis of the α_1-β subunit interaction of voltage-gated Ca^{2+} channels. *Nature* **429:** 675–680.

Cornilescu, G., Delaglio, F., and Bax, A. 1999. Protein backbone angle restraints from searching a database for chemical shift and sequence homology. *J. Biomol. NMR* **13:** 289–302.

Dalton, S., Takahashi, S.X., Miriyala, J. and Colecraft, H.M. 2005. A single $Ca_v\beta$ can reconstitute both trafficking and macroscopic conductance of voltage-dependent Ca^{2+} channels. *J. Physiol.* **567 (Pt. 3):** 757–769.

Delaglio, F., Grzesiek, S., Vuister, G.W., Zhu, G., Pfeifer, J., and Bax, A. 1995. NMRPipe: A multidimensional spectral processing system based on UNIX pipes. *J. Biomol. NMR* **6:** 277–293.

Edelhoch, H. 1967. Spectroscopic determination of tryptophan and tyrosine in proteins. *Biochemistry* **6:** 1948–1954.

Hanlon, M.R., Berrow, N.S., Dolphin, A.C., and Wallace, B.A. 1999. Modelling of a voltage-dependent Ca^{2+} channel β subunit as a basis for understanding its functional properties. *FEBS Lett.* **445:** 366–370.

Helgstrand, M., Kraulis, P., Allard, P., and Hard, T. 2000. Ansig for Windows: An interactive computer program for semiautomatic assignment of protein NMR spectra. *J. Biomol. NMR* **18:** 329–336.

Helton, T.D., and Horne, W.A. 2002. Alternative splicing of the β_4 subunit has α_1 subunit subtype-specific effects on Ca^{2+} channel gating. *J. Neurosci.* **22:** 1573–1582.

Helton, T.D., Kojetin, D.J., Cavanagh, J., and Horne, W.A. 2002. Alternative splicing of a β_4 subunit proline-rich motif regulates voltage-dependent gating and toxin block of $Ca_v2.1$ Ca^{2+} channels. *J. Neurosci.* **22:** 9331–9339.

Johnson, B.A. and Blevins, R.A. 1994. NMRView: A computer program for the visualization and analysis of NMR data. *J. Biomol. NMR* **4:** 603–614.

Kuboniwa, H., Grzesiek, S., Delaglio, F., and Bax, A. 1994. Measurement of H^N-H^α J couplings in Ca^{2+}-free calmodulin using new 2D and 3D water-flip-back methods. *J. Biomol. NMR* **4:** 871–878.

Lipscombe, D. 2005. Neuronal proteins custom designed by alternative splicing. *Curr. Opin. Neurobiol.* **15:** 358–363.

Maltez, J.M., Nunziato, D.A., Kim, J., and Pitt, G.S. 2005. Essential $Ca_v\beta$ modulatory properties are AID-independent. *Nat. Struct. Mol. Biol.* **12:** 372–377.

McGee, A.W., Dakoji, S.R., Olsen, O., Bredt, D.S., Lim, W.A., and Prehoda, K.E. 2001. Structure of the SH3-guanylate kinase module from PSD-95 suggests a mechanism for regulated assembly of MAGUK scaffolding proteins. *Mol. Cell.* **6:** 1291–1301.

McGee, A.W., Nunziato, D.A., Maltez, J.M., Prehoda, K.E., Pitt, G.S., and Bredt, D.S. 2004. Calcium channel function regulated by the SH3-GK module in β subunits. *Neuron* **42:** 89–99.

McIntosh, L.P. and Dahlquist, F.W. 1990. Biosynthetic incorporation of ^{15}N and ^{13}C for assignment and interpretation of nuclear magnetic resonance spectra of proteins. *Q. Rev. Biophys.* **23:** 1–38.

Opatowsky, Y., Chen, C.C., Campbell, K.P., and Hirsch, J.A. 2004. Structural analysis of the voltage-dependent Ca^{2+} channel β subunit. *Neuron* **42:** 387–399.

Pragnell, M., De Waard, M., Mori, Y., Tanabe, T., Snutch, T.P., and Campbell, K.P. 1994. Calcium channel β subunit binds to a conserved

motif in the I–II cytoplasmic linker of the α_1 subunit. *Nature* **368:** 67–70.

Richards, M.W., Butcher, A.J., and Dolphin, A.C. 2004. Ca^{2+} channel β-subunits: Structural insights AID our understanding. *Trends Pharmacol. Sci.* **25:** 626–632.

Ruth, P., Rohrkasten, A., Biel, M., Bosse, E., Regulla, S., Meyer, H.E., Flockerzi, V., and Hofmann, F. 1989. Primary structure of the β subunit of the DHP-sensitive Ca^{2+} channel from skeletal muscle. *Science* **245:** 1115–1118.

Van Petegem, F., Clark, K.A., Chatelain, F.C., and Minor Jr., D.L. 2004. Structure of a complex between a voltage-gated Ca^{2+} channel β subunit and an α subunit domain. *Nature* **429:** 671–675.

White, J.V., Stultz, C.M., and Smith, T.F. 1994. Protein classification by stochastic modeling and optimal filtering of amino-acid sequences. *Math. Biosci.* **119:** 35–75.

Wishart, D.S. and Case, D.A. 2001. Use of chemical shifts in macromolecular structure determination. *Methods Enzymol.* **338:** 3–34.